Effects of sub-seasonal variability on seasonal-to-interannual Indian Ocean meridional heat transport

D. J. Halkides,[1] Weiqing Han,[2] Tong Lee,[1] and Yukio Masumoto[3,4]

Received 26 March 2007; revised 4 May 2007; accepted 15 May 2007; published 22 June 2007.

[1] Numerical experiments using the Hybrid Coordinate Ocean Model are performed to examine atmospheric intraseasonal oscillation (ISO) effects on seasonal-to-interannual meridional heat transport (Q_v) in the tropical Indian Ocean. Analysis focuses on the equator and 14.5°S, latitudes associated with the cross-equatorial and southern subtropical meridional cells. ISOs alter seasonal Q_v anomaly (Q_v^*) at these latitudes by a-few-hundredths PW up to 2–3 tenths PW. On interannual timescales, heat transport anomaly (Q_v') induced by ISOs tends to reinforce (correlates positively with) the total Q_v' signal. ISO winds can induce interannual Q_v' up to 0.15 PW, comparable to the maximum amplitude of the Q_v' signal. Net effects of atmospheric ISOs can account for ~30% of Q_v' in some years; in others, ISO contributions are insignificant. Wind stress (via momentum flux) and wind speed (via turbulent heat fluxes and vertical mixing) play notable roles in ISO effects on Q_v^* and in some years on Q_v'. **Citation:** Halkides, D. J., W. Han, T. Lee, and Y. Masumoto (2007), Effects of sub-seasonal variability on seasonal-to-interannual Indian Ocean meridional heat transport, *Geophys. Res. Lett.*, *34*, L12605, doi:10.1029/2007GL030150.

1. Introduction

[2] Despite extensive progress in recent years toward improved understanding of interannual variability in the tropical Indian Ocean (IO), the intrinsic (non-ENSO) component of that variability and how it is affected by meridional heat transport (Q_v) are not well-understood. This is due to insufficient understanding of Q_v variability on a wide range of timescales. Cross-scale rectification of atmospheric intraseasonal oscillations (ISOs), i.e., the Madden-Julian Oscillation (30–90 day periods) [*Madden and Julian*, 1971] and the quasi-biweekly oscillation [*Chatterjee and Goswami*, 2004], into low-frequency ocean variability may contribute to low-frequency Q_v variability. Historically, ocean general circulation model (OGCM) studies on interannual variability used monthly forcings. Today, OGCMs are driven by higher frequency forcings to achieve more accurate depiction of the ocean state; yet, ISO contributions to seasonal-to-interannual Q_v have not been quantified.

[3] It is believed that the upper-IO heat balance is achieved by shallow meridional circulations known as the Cross-Equatorial Cell (CEC) [*Miyama et al.*, 2003; *Schott et al.*, 2004] and the Southern Subtropical Cell (SSTC) [*Schott et al.*, 2004]. The CEC connects upwelling zones in the northern IO to subduction zones in the southeastern IO via a southward, cross-equatorial branch concentrated in the upper 50 m depth and northward bulk-flow of cooler thermocline water (a schematic of the meridional circulation is given by *Lee* [2004]). CEC variability accounts for a significant portion of IO cross-equatorial heat transport (CEHT), which is hypothesized to be associated with the Asian-Australian monsoon; and, CEHT variability associated with the Tropical Biennial Oscillation may play a role in Indian Ocean Zonal Dipole Mode (IOZDM) development [*Loschnigg et al.*, 2003]. The SSTC is maintained by open-ocean upwelling at 2–12°S [e.g., *McCreary et al.*, 1993; *Murtugudde et al.*, 1998; *Xie et al.*, 2002], which is driven by Ekman divergence associated with local wind stress curl, and is sensitive to IOZDM variability [e.g., *Webster et al.*, 1999; *Xie et al.*, 2002]. Below, we examine Q_v in the region associated with the superimposed SSTC and CEC at 14.5°S. This latitude lies south of the maximum open-ocean upwelling where the Ekman pumping velocity (w_e) is near zero [*Han et al.*, 2006b], such that it separates upwelling that drives the SSTC from subtropical subduction.

[4] Understanding seasonal-to-interannual variations in Q_v strength in regions associated with the CEC and SSTC is important, as these circulations directly affect the IO heat balance and thus modify SST and climate predictability (see *Schott et al.* [2004] for a review). Existing studies address ISO rectification into seasonal-to-interannual variability of zonal current, zonal heat transport and SST in the tropical Pacific and IO [*Kessler and Kleeman*, 2000; *Han et al.*, 2004; *Waliser et al.*, 2003, 2004]. Yet, how ISOs affect IO Q_v on seasonal-to-interannual timescales is uncertain. Here, OGCM experiments are performed to estimate ISO impacts on seasonal-to-interannual IO Q_v, focusing on latitudes associated with the CEC and SSTC. The results have implications for more accurate ocean/climate model simulations and prediction.

2. Model Description

[5] We use the Hybrid Coordinate Ocean Model (HYCOM) [*Bleck*, 2002] configured to the IO north of 30°S, with 0.5° × 0.5° horizontal resolution, realistic bottom topography and 18 vertical layers [*Han et al.*, 2004]. It is forced with 3-day mean atmospheric fields for January 1993–November 2004. ISOs are most energetic at periods near two weeks and 30–90 days, so 3-day averaged forcing is sufficient for our purposes. Wind stress and wind

[1]Earth Sciences, Jet Propulsion Laboratory, California Institute of Technology, Pasadena, California, USA.
[2]Department of Atmospheric and Oceanic Sciences, University of Colorado, Boulder, Colorado, USA.
[3]Institute of Observational Research for Global Change, Japan Agency for Marine-Earth Science and Technology, Yokosuka, Japan.
[4]Department of Earth and Planetary Sciences, University of Tokyo, Tokyo, Japan.

0094-8276/07/2007GL030150$05.00

speed are from the ECMWF 40-Year Re-analysis (ERA-40) for January 1993–June 1999, after which winds are from NASA's Quick Scatterometer (QuikSCAT) satellite. The QuikSCAT winds transition smoothly from ERA40 winds in 1999. ERA-40 air temperature and humidity are used until August 2001, after which NCEP-NCAR reanalysis products are used. Solar and long-wave radiation fluxes from the International Satellite Cloud Climatology Project Flux Dataset (ISCCP-FD) [*Zhang et al.*, 2004] are used until August 2001, after which these are calculated via linear regression of OLR data using coefficients derived from ISCCP data. CDC Merged Analysis of Precipitation (CMAP) data is used for the entire period. See *Han et al.* [2006a, 2007] for details on the model spin-up and forcing feasibility.

[6] Meridional heat flux from the surface through layer *d* can be calculated as follows:

$$Q_v^d = c_p \int_{i=1}^{i=d} \int \rho_i v_i T_i dx dz_i \quad (1)$$

Here, i = {1...d} is layer number; a value for *d* of 18 represents the full water column. Specific heat c_p = 3994 J (kg °C)$^{-1}$, ρ is layer density, v is meridional velocity, T is temperature, dx is horizontal resolution, dz is layer thickness and ρvT at a given latitude is integrated in longitude and in depth from the surface to *d*. Near the entrance of the Indonesian throughflow (ITF), the model uses a sponge layer in which temperature and salinity are relaxed to the observed seasonal cycles [*Levitus and Boyer*, 1994; *Levitus et al.*, 1994]. As a result, there is no net volume flux associated with the ITF. Therefore, when equation (1) is integrated over the full column depth, the temperature flux represents heat transport, because there is no net volume flux across any section. We find the mean and seasonal cycle of meridional heat transport for the water column (Q_v^{18}) are nearly identical to those for Q_v^d integrated to layer 15 (Q_v^{15}). So hereafter, we only discuss Q_v^{15}, using a simplified notation of Q_v, and Q_v will be referred to as meridional heat transport.

[7] ISOs can induce seasonal-to-interannual Q_v variability via nonlinearities in the system. These nonlinearities are apparent when each variable in equation (1) is expanded into mean, seasonal, interannual and intraseasonal components; e.g., $v_i = \bar{v}_i + v_i^* + v_i' + v_i''$, where $\bar{v}_i$ is the mean, v_i^* is the seasonal cycle, v_i' is interannual variability and v_i'' is intraseasonal variability of v in layer *i*. Similar expressions can be written for all equation (1) variables. When equation (1) is expanded, it is clear seasonal (Q_v^*) and interannual (Q_v') variability in Q_v can not be separated from intraseasonal variability in the system. Expansion of Q_v shows intraseasonal transport of seasonal-to-interannual temperature variability ($v''T^*$ and $v''T'$), seasonal-to-interannual transport of intraseasonal temperature variability (v^*T'' and $v'T''$) and intraseasonal transport of intraseasonal temperature ($v''T''$) are the main processes through which ISOs cause seasonal-to-interannual Q_v. So ISO wind stress, which drives v'' and affects temperature via horizontal advection and Ekman upwelling, and ISO wind speed, which affects ocean temperature via turbulent heat fluxes and mixing, may contribute significantly to seasonal-to-interannual Q_v.

[8] These runs are used to estimate ISO contributions to Q_v^* and Q_v', and associated mechanisms: (1) the main run (MR), forced by forcing fields described above; (2) test run T0, for which intraseasonal variability is removed from all forcings via a 105-day low-pass Lanczos filter; (3) run T1, for which intraseasonal variability is removed from wind stress; and (4) run T2, for which intraseasonal variability is removed from wind stress and wind speed forcings. Solution MR-T0 estimates the response to all atmospheric ISOs. Solution MR-T1 is the response to ISO wind stress. Solution MR-T2 is the combined response to ISO wind stress and wind speed. Solution T1-T2 approximates ISO wind speed effects.

3. Results

[9] To evaluate HYCOM's suitability for our work, Figure 1a (Figure 1b) compares 3-day zonal (meridional) MR current anomaly (time mean removed) at the equator and 90°E averaged over HYCOM isopycnal layer 2 (which has a mean depth near 50 m) to Acoustic Doppler Current Profiler (ADCP) [*Masumoto et al.*, 2005] measurements near 50 m. The simulated and observed zonal (meridional) currents yield a correlation coefficient of $r = 0.7$ ($r = 0.34$), which exceeds the 99.5% student-T confidence level. Comparable HYCOM-ADCP *r*-values are found throughout the water column. HYCOM reasonably simulates zonal current, but the correlation between HYCOM and ADCP meridional current is not as good. This is because the meridional current is dominated by 12–15 day oscillations [*Miyama et al.*, 2006]. These frequencies are higher than those of the zonal current, so small phase-shifts affect *r* more significantly. Phase shifts may arise from inaccuracy of surface forcings in resolving high frequency variability, or be due to linear interpolation of missing values in observed current (high frequency variability increases the possibility that interpolated values are inaccurate, reducing *r*). Yet, both the timescales of variability and standard deviation of MR v-current are comparable to those observed ($\sigma_{MR} = 0.15$ and $\sigma_{ADCP} = 0.19$ m/s). Furthermore, the annual harmonics of the simulated and ADCP v-currents in the upper IO agree well (Figure 1c). This suggests HYCOM can estimate ISO impacts on low-frequency Q_v, despite reduction of the correlation of MR v-current with observations by small phase shifts. Note that, we also compared HYCOM current with a Kalman filter and smoother assimilation product from the Estimating the Circulation and Climate of the Ocean (ECCO) project (available at http://ecco.jpl.nasa.gov/external) [*Fukumori*, 2002, 2006]. HYCOM-ECCO current correlation values at (EQ, 90°E; not shown) are similar to those for HYCOM and ADCP currents. Lastly, included in Figure 1 (in red) are corresponding u- and v-current time series from run T0, for which intraseasonal variability was removed from all atmospheric forcings. A comparison of the T0 and MR currents demonstrates the net effect of ISOs on MR u- and v-current anomalies and on the MR v-current annual harmonic.

[10] Figures 2a and 2d show monthly seasonal cycles (time means removed) of the meridional transport streamfunctions (Ψ_V^*, where $\Psi_V = \int_{i=1}^{i=d} \int v_i dx dz_i$) at the equator and 14.5°S (y-axis values are derived via cubic Spline-

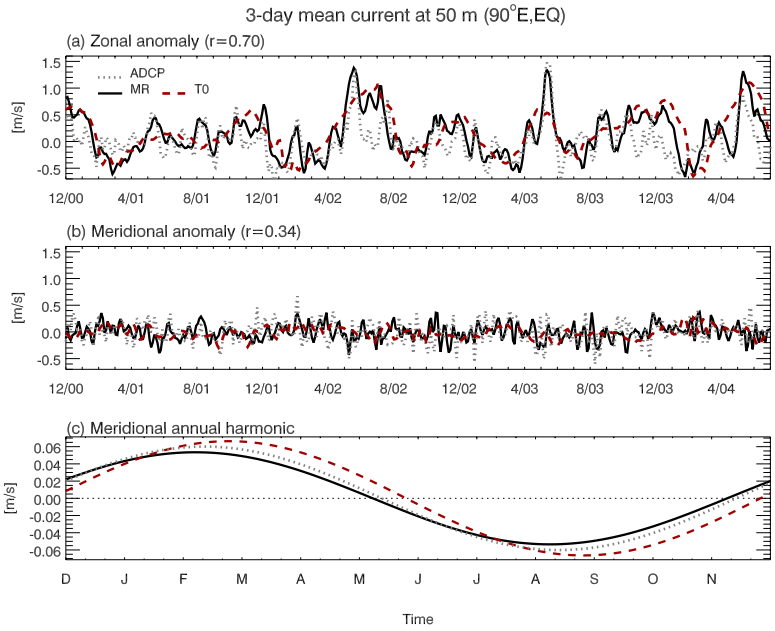

Figure 1. Simulated (black solid) and observed (gray dotted) 3-day near-surface current anomaly at the equator, 90°E in m/s: (a) zonal current, (b) meridional current, and (c) annual harmonic of meridional current. ADCP indices are taken near 50 m depth; MR indices are averaged over HYCOM isopycnal layer 2, which has a mean near 50 m. Dashed red lines represent analogous currents from run T0, for which all ISOs were removed from the atmospheric forcings. Differences between the MR and T0 time-series represent the effects of ISOs on MR current anomalies.

interpolation from the monthly mean depths of HYCOM isopycnal layer interfaces). In Figure 2a, the near-surface cross-equatorial roll [e.g., *Wacongne and Pacanowski*, 1996; *Lee and Marotzke*, 1998; *Miyama et al.*, 2003], which is northward in spring-fall, is visible near the surface. Upper ocean volume transport across the equator is concentrated at 40–200 m depth with a maximum near 50 m (where streamlines are densest), and it flows southward (northward) from mid-April through October (November to mid-April). The direction of transport reverses (depth integrated transport decreases) at around 200 m depth. At 14.5°S (Figure 2d), meridional flow reverses direction at ~750 m depth. This structure of Ψ_V^* with depth is similar to that presented by *Lee and Marotzke* [1998] for January and July at the equator and 15°S. Figures 2b and 2e display monthly MR Q_v^* time-series and the corresponding boreal spring-fall (April through October) and winter (remainder of the year) mean Q_v^* at the equator and 14.5°S for years 1993–2003 (2004 is omitted due to an incomplete year). The maximum amplitudes of Q_v^* are about 1.5 PW and 1.3 PW at the equator and at 14.5°S, respectively (where amplitude is half the difference between the maximum and minimum monthly Q_v^*). The amplitudes at the equator and 14.5°S are comparable to what is reported in prior studies [e.g., *Hsiung et al.*, 1989; *Lee and Marotzke*, 1998; *Jayne and Marotzke*, 2001; *Chirokova and Webster*, 2006]. Thus we believe HYCOM reasonably simulates Q_v^* at the equator and 14.5°S, locations where the CEC and SSTC are estimated. *Han et al.* [2006a, 2007] include further validation of HYCOM for study of ISO effects on the IO.

[11] Figures 2b and 2e also show monthly MR-T0 Q_v^* (dotted line) at the equator and 14.5°S. This illustrates that ISO-induced Q_v^* tends to be small relative to Q_v^* itself (solid gray line), although it can be significant in some instances, i.e., in October, ISOs enhance southward equatorial Q_v^* by between 0.2–0.3 PW. Such occurrences should be noted in considering possible ISO rectification into low frequency variability. Note Q_v^* and its relative sensitivity to ISOs vary some with latitude, but in general ISOs tends to affect Q_v^* in the equatorial and southern tropics by between a-few hundredths and 2–3 tenths PW. Additionally, comparison of MR-T0, MR-T1 and MR-T2 Q_v^* (not shown) indicates that what effects ISOs do have on the Q_v^* signal are dominated by ISO wind stress effects on momentum flux, and that in some months ISO wind speed effects on turbulent fluxes and mixing partially compensate for wind stress-induced Q_v^*.

[12] To depict ISO effects on interannual scales, Figures 2c and 2f show MR $Q_v' = Q_v - \bar{Q}_v - Q_v^* - Q_v''$ for each year (solid gray line) and Q'_v caused by all ISOs (MR-T0), ISO wind stress (MR-T1) and ISO wind stress and wind speed (MR-T2) at the equator and 14.5°S during 1994–2002 (1993 and 2003/04 are omitted due to filter edge-effects). Error bars for these curves, defined by the standard statistical error of each time series, are also included in Figures 2c and 2f (except for MR-T1, the amplitude of which is small) to illustrate the statistical significance of ISO-induced Q'_v and the contributions by wind stress/speed. The relative importance of ISO wind stress and wind speed to total ISO-driven Q'_v varies. In some years, the response to ISOs respective to Q'_v is large and there are distinct differences between the total ISO-induced Q'_v and the wind stress/speed contributions. Figures 2c and 2f indicate some correlation between Q'_v and ISO-induced Q'_v, especially at the equator, e.g., when equatorial Q'_v is large and northward (in 1995, 1998, 2001), the ISO contribution also tends to be northward and statistically significant (i.e., statistically different from zero). Generally, ISOs appear to reinforce Q'_v,

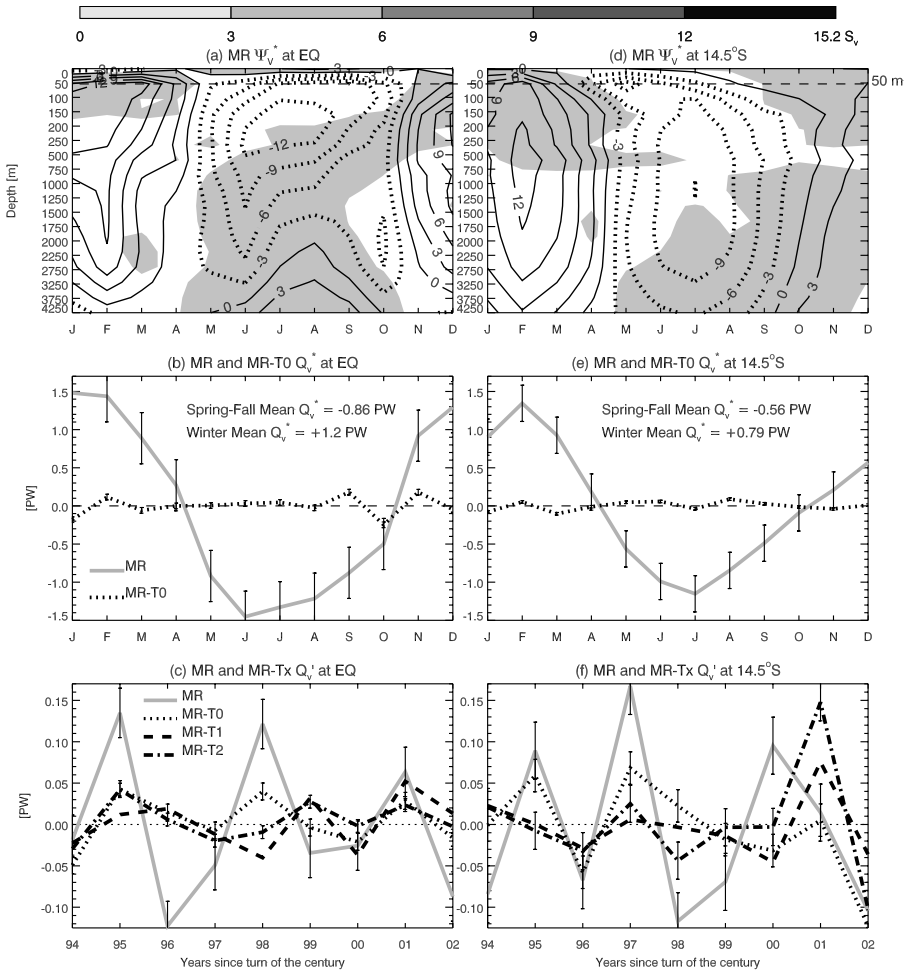

Figure 2. (a, d) Monthly seasonal cycles (time mean removed) of MR meridional transport streamfunctions (Ψ_V^*) at the equator and 14.5°S for January 1993–December 2003. Solid contours (dotted contours) are positive (negative) Ψ_V^* values with a 3 S_v interval. Since Ψ_V^* at each depth is integrated vertically from the surface and flow is perpendicular to the page, gray (white) shading is used to indicate northward (southward) flow. (b, e) MR (solid gray) and MR-T0 (dotted) Q_v^*, as well as MR spring–fall (April–October) and winter (remainder of year) mean Q_v^* at the equator and 14.5°S. (c, f) Q_v' for each year from the MR (solid gray) and MR-Tx solutions at the equator and 14.5° during 1994–2002. The MR-Tx solutions show Q_v caused by corresponding ISOs. Error bars in Figures 2b, 2c, 2e, and 2f represent standard error for MR and standard error of the difference for MR-Tx.

but there are exceptions, e.g., equatorial Q_v' in 1996 is large but the corresponding ISO contribution is small, and at 14.5°S in 2000 Q_v' and its ISO component have opposite signs.

[13] At the equator, the maximum amplitude of MR Q_v' during our time period is nearly 0.14 PW and occurs in 1995. Intraseasonal wind-driven processes account for nearly 32% of Q_v' in this year, and most of this contribution appears to be due to wind-speed effects on turbulent heat fluxes and mixing. Similarly, in 1998, combined ISO-driven effects account for 33% of a northward Q_v' of ≈0.12 PW; yet here, the response to ISO wind effects is negative, indicating ISOs in surface radiation fluxes and/or precipitation are important to the ISO Q_v' contribution in this year. In 2000 and 2001, MR Q_v' is somewhat smaller, but appears to be closely related to ISO wind stress.

[14] At 14.5°S, combined atmospheric ISOs have significant effects on Q_v' in 1995, 1996, 1997 and 2002. ISO wind-induced Q_v' is large in 1996, 1998, 2001 and 2002. Note that in 1994, 1997 and 2001, the Q_v' response to ISO winds (MR-T2) is northward. Both 1994 and 1997 were years in which strong positive IOZDM events occurred, such that interannual SSTA in the western (southeastern) tropics was positive (negative). A weaker positive west–east temperature gradient was also present in 2001, when the response of Q_v' to ISO winds is greatest (0.15 PW). On the other hand, southward Q_v' is induced by total ISOs at 14.5°S in 1996; and, in 1998, the Q_v' response to ISO winds is strongly southward. Both 1996 and 1998 were negative IOZDM years, when the dipole-like SSTA gradient was reversed. This may imply ISO-induced Q_v' is linked to IOZDM behavior. This is not surprising, as the IOZDM can modulate ISOs [*Shinoda and Han*, 2005]. Lastly, in 1995 and 2001 ISO radiation fluxes and/or precipitation appear to make important contributions to net ISO-induced Q_v', since large differences exist between the MR-T0 and MR-T2 solutions for Q_v'.

[15] Here, we report the most clear-cut ISO-impacts on Q_v' at the equator and 14.5°S. More work must be done to confirm any relationship between the IOZDM and ISO-

driven Q_v, to better quantify processes contributing to ISO-induced Q_v' and to determine how climatic conditions affect system sensitivity to ISOs. This work, in progress, is beyond the scope of this note.

4. Summary

[16] HYCOM is used to estimate atmospheric ISO effects on seasonal-to-interannual Q_v in the tropical IO, to improve understanding of the IO heat balance. ISOs can alter Q_v^* in the equatorial and southern tropics by up to $\sim$0.2–0.3 PW, but typically have a smaller effect. ISO wind-driven processes dominate ISO effects on Q_v^*. ISO-induced Q_v' and the relative importance of contributing mechanisms varies between years. Total ISO-induced Q_v' can account for $\sim$30% of Q_v' in some years. ISO winds alone can cause Q_v' of up to 0.15 PW–close to the amplitude of Q_v' itself. A link may exist between ISO-driven Q_v' and the IOZDM in the southern tropics. In some years, processes driven by ISO radiation fluxes and/or rainfall may dominate MR-T0 Q_v'. Further work is needed to determine how climate conditions affect system sensitivity to ISOs and to quantify feedbacks to climate. This includes separation of Q_v associated with the MJO and quasi-biweekly winds and quantification of processes associated with ISO-induced Q_v when wind effects are small. Once ISO contributions to Q_v are understood, implications for SST and climate predictability can be examined.

[17] **Acknowledgments.** Thanks to the JPL ECCO team for providing their Kalman filter assimilation products. D.J. Halkides and Weiqing Han are supported by NSF OCE-0136836, NSF OCE-0452917, and NASA Ocean Vector Winds Program award 1283568. The research described above was partially carried out at the Jet Propulsion Laboratory, California Institute of Technology, under a contract with NASA.

References

Bleck, R. (2002), An oceanic general circulation model framed in hybrid isopycnic-Cartesian coordinates, *Ocean Modell.*, *4*, 55–88.

Chatterjee, P., and B. N. Goswami (2004), Structure, genesis and scale selection of the tropical quasi-biweekly mode, *Q. J. R. Meteorol. Soc.*, *130*, 1171–1194, doi:10.1256/qj.03.133.

Chirokova, G., and P. J. Webster (2006), Interannual variability of Indian Ocean heat transport, *J. Clim.*, *19*, 1013–1031.

Fukumori, I. (2002), A partitioned Kalman filter and smoother, *Mon. Weather Rev.*, *130*, 1370–1383.

Fukumori, I. (2006), What is data assimilation really solving, and how is the calculation actually done?, in *Ocean Weather Forecasting: An Integrated View of Oceanography*, edited by E. P. Chassignet and J. Verron, pp. 317–342, Springer, New York.

Han, W., P. J. Webster, R. Lukas, P. Hacker, and A. Hu (2004), Impact of atmospheric intraseasonal variability in the Indian Ocean: Low-frequency rectification in equatorial surface current and transport, *J. Phys. Oceanogr.*, *34*, 1350–1372.

Han, W., T. Shinoda, L. L. Fu, and J. P. McCreary (2006a), Impact of atmospheric intraseasonal oscillations on the Indian Ocean dipole during the 1990s, *J. Phys. Oceanogr.*, *36*, 670–690, doi:10.1175/JPO2892.1.

Han, W., G. A. Meehl, and A. Hu (2006b), Interpretation of tropical thermocline cooling in the Indian and Pacific oceans during recent decades, *Geophys. Res. Lett.*, *33*, L23615, doi:10.1029/2006GL027982.

Han, W., D. Yuan, W. T. Liu, and D. J. Halkides (2007), Intraseasonal variability of Indian Ocean sea surface temperature during boreal winter: Madden-Julian Oscillation versus submonthly forcing and processes, *J. Geophys. Res.*, *112*, C04001, doi:10.1029/2006JC003791.

Hsiung, J., R. E. Newell, and T. Houghtby (1989), The annual cycle of oceanic heat storage and oceanic meridional heat transport, *Q. J. R. Meteorol. Soc.*, *115*, 1–28.

Jayne, S. R., and J. Marotzke (2001), The dynamics of ocean heat transport variability, *Rev. Geophys.*, *39*(3), 385–411.

Kessler, W. S., and R. Kleeman (2000), Rectification of the Madden-Julian Oscillation into the ENSO cycle, *J. Clim.*, *13*, 3560–3575.

Lee, T. (2004), Decadal weakening of the shallow overturning circulation in the South Indian Ocean, *Geophys. Res. Lett.*, *31*, L18305, doi:10.1029/2004GL020884.

Lee, T., and J. Marotzke (1998), Seasonal cycles of meridional overturning and heat transport of the Indian Ocean, *J. Phys. Oceanogr.*, *28*, 923–943.

Levitus, S., and T. P. Boyer (1994), *World Ocean Atlas 1994*, vol. 4, *Temperature*, *NOAA ATLAS NESDIS 4*, 117 pp., U.S. Dep. of Commer., Washington, D. C.

Levitus, S., R. Burgett, and T. P. Boyer (1994), *World Ocean Atlas 1994*, vol. 3, *Salinity*, *NOAA ATLAS NESDIS 3*, 99 pp., U.S. Dep. of Commer., Washington, D. C.

Loschnigg, J., G. A. Meehl, P. J. Webster, J. M. Arblaster, and G. P. Compo (2003), The Asian monsoon, the tropospheric biennial oscillation, and the Indian Ocean zonal mode in the NCAR CSM, *J. Clim.*, *16*, 1617–1642.

Madden, R. A., and P. R. Julian (1971), Detection of a 40–50 day oscillation in the zonal wind in the tropical Pacific, *J. Atmos. Sci.*, *28*, 702–708.

Masumoto, Y., H. Hase, Y. Kuroda, H. Matsuura, and K. Takeuchi (2005), Intraseasonal variability in the upper layer currents observed in the eastern equatorial Indian Ocean, *Geophys. Res. Lett.*, *32*, L02607, doi:10.1029/2004GL021896.

McCreary, J. P., Jr., P. K. Kundu, and R. L. Molinari (1993), A numerical investigation of dynamics, thermodynamics and mixed-layer processes in the Indian Ocean, *Prog. Oceanogr.*, *31*, 181–244.

Miyama, T., J. P. McCreary Jr., T. G. Jensen, J. Loschnigg, S. Godfrey, and A. Ishida (2003), Structure and dynamics of the Indian Ocean cross-equatorial cell, *Deep Sea Res., Part II*, *50*, 2023–2047.

Miyama, T., J. P. McCreary, D. Sengupta, and R. Senan (2006), Dynamics of biweekly oscillations in the equatorial Indian Ocean, *J. Phys. Oceanogr.*, *36*, 827–846.

Murtugudde, R. G., S. R. Signorini, J. R. Christian, A. J. Busalacchi, C. R. McClain, and J. Picaut (1998), Ocean color variability of the tropical Indo-Pacific basin observed by SeaWiFS during 1997–1998, *J. Geophys. Res.*, *104*(C8), 18,351–18,366.

Schott, F. A., J. P. McCreary, and G. C. Johnson (2004), Shallow overturning circulations of the tropical-subtropical oceans, in *Earth's Climate: The Ocean-Atmosphere Interaction*, *Geophys. Monogr. Ser.*, vol. 147, edited by C. Wang, S-.P. Xie, and J. A. Carton, pp. 261–304, AGU, Washington, D. C.

Shinoda, T., and W. Han (2005), Influence of Indian Ocean dipole on atmospheric subseasonal variability, *J. Clim.*, *18*, 3891–3909.

Wacongne, S., and R. C. Pacanowski (1996), Seasonal heat transport in a primitive equation model of the tropical Indian Ocean, *J. Phys. Oceanogr.*, *26*, 2666–2699.

Waliser, D. E., R. Murtugudde, and L. E. Lucas (2003), Indo-Pacific Ocean response to atmospheric intraseasonal variability: 1. Austral summer and the Madden-Julian Oscillation, *J. Geophys. Res.*, *108*(C5), 3160, doi:10.1029/2002JC001620.

Waliser, D. E., R. Murtugudde, and L. E. Lucas (2004), Indo-Pacific Ocean response to atmospheric intraseasonal variability: 2. Boreal summer and the Intraseasonal Oscillation, *J. Geophys. Res.*, *109*, C03030, doi:10.1029/2003JC002002.

Webster, P. J., A. M. Moore, J. P. Loschnigg, and R. R. Leben (1999), Coupled ocean–atmosphere dynamics in the Indian Ocean during 1997–98, *Nature*, *401*, 356–359.

Xie, S.-P., H. Annamalai, F. Schott, and J. P. McCreary Jr. (2002), Origin and predictability of South Indian Ocean climate variability, *J. Clim.*, *15*, 864–878.

Zhang, Y., W. B. Rossow, A. A. Lacis, V. Oinas, and M. I. Mishchenko (2004), Calculation of radiative fluxes from the surface to top of atmosphere based on ISCCP and other global data sets: Refinements of the radiative transfer model and the input data, *J. Geophys. Res.*, *109*, D19105, doi:10.1029/2003JD004457.

D. J. Halkides and T. Lee, Earth Sciences, Jet Propulsion Laboratory, JPL Mail Stop 300-323, 4800 Oak Grove Drive, Pasadena, CA 91109, USA. (halkides@jpl.nasa.gov)

W. Han, Department of Atmospheric and Oceanic Sciences, University of Colorado, Campus Box 311, Boulder, CO 80309, USA. (whan@enso.colorado.edu)

Y. Masumoto, Institute of Observational Research for Global Change, Japan Agency for Marine-Earth Science and Technology, 2-15 Natsushima-cho, Yokosuka, Kanagawa 237-0061, Japan.